THE JOURNAL OF PHYSICAL CHEMISTRY A

Article

Cite This: J. Phys. Chem. A 2019, 123, 4034−4047

pubs.acs.org/JPCA

Donor Halogenation Effects on Electronic Structures and Electron Process Rates of Donor/C_{60} Heterojunction Interface: A Theoretical Study on F_nZnPc (n = 0, 4, 8, 16) and Cl_nSubPc (n = 0, 6)

Rui-Rong Bai,[†,‡] Cai-Rong Zhang,*[,†,‡,§] You-Zhi Wu,[†] Yu-Lin Shen,[∥] Zi-Jiang Liu,[⊥] and Hong-Shan Chen[§]

[†]State Key Laboratory of Advanced Processing and Recycling of Non-ferrous Metals and [‡]Department of Applied Physics, Lanzhou University of Technology, Lanzhou, Gansu 730050, China

[§]College of Physics and Electronic Engineering, Northwest Normal University, Lanzhou, Gansu 730070, China

[∥]Gansu Computing Center, Lanzhou, Gansu 730000, China

[⊥]Department of Physics, Lanzhou City University, Lanzhou, Gansu 730070, China

Supporting Information

ABSTRACT: Molecular engineering is significantly important for developing electron donor and acceptor materials of active layers in organic photovoltaics (OPVs). The OPVs based on halogenated donors frequently produced high power conversion efficiencies. Here, based upon density functional theory calculations with optimally tuned range separation parameters and solid polarization effects, we studied the effects of donor halogenation on molecular geometries, electronic structures, excitation, and spectroscopic properties for F_nZnPc (n = 0, 4, 8, 16) and Cl_nSubPc (n = 0, 6) monomers and the complexes with C_{60} as well as the photoinduced direct charge transfer (CT), exciton dissociation (ED), and charge recombination (CR) processes that were described by rate constants calculated using Marcus theory. The tiny differences of the molecular orbital energy gap, excitation, and spectroscopic properties of F_nZnPc (n = 0, 4, 8, 16) and Cl_nSubPc (n = 0, 6) monomers suggest that halogenation cannot effectively tune the electronic and optical gap but the significant decrease of molecular orbital energies support the idea that halogenation has a remarkable influence on the energy level alignment at heterojunction interfaces. The halogenation also enhances intermolecular binding energies between C_{60} and donors and increases the CT excitation energies of donor/C_{60} complexes, which are favorable for improving open circuit voltage. Furthermore, for F_nZnPc/C_{60} (n = 0, 4, 8, 16) and SubPc/C_{60} (n = 0, 6) complexes, the CR rates dramatically decrease (several orders) with increasing number of halogen atoms (except for F_{16}ZnPc/C_{60}), meaning suppression of CR processes by halogenation. As for the special case of F_{16}ZnPc/C_{60}, it underlines the importance of fluorination degree in molecular design of donor materials. This study provides a theoretical understanding of the halogenation effects of donors in OPVs and may be helpful in molecular design for electron donor materials.

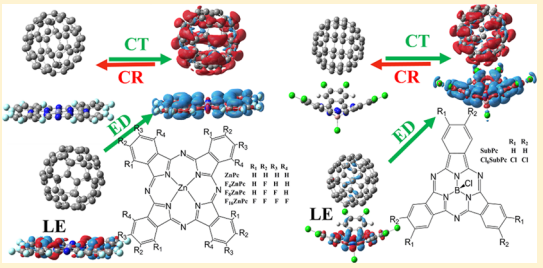

1. INTRODUCTION

As emerging photovoltaic technology and equipment, organic photovoltaics are promising due to their low cost, flexibility, light weight, and other merits. A power conversion efficiency (PCE) of 17.3% was achieved by a two-terminal monolithic solution-processed tandem OPV with PBDB-T/F-M and PTB7-Th:O6T-4F/PC_{71}BM as active layers.[1] Design and synthesis of novel materials, optimizing processing conditions and device architectures, are effective routes to improve the PCE of OPVs.[2] Qualitatively, the photon-to-electricity conversion processes in OPVs include photon absorption and exciton generation, exciton diffusion and dissociation, charge separation and free charge carrier generation, and charge transport and collection at the electrode.[3] Most of the electron processes involved in photon-to-electricity conversion occur in the active layer, which contains a heterojunction composed of electron donor and acceptor materials.[4,5] Hence, developing novel materials for the active layer in OPVs plays a critical role in PCE improvement.

Molecular engineering is significantly important for developing electron donor and acceptor materials of organic heterojunctions in OPV active layers[6,7] because molecular structures can effectively tune electronic structures, light-harvesting abilities, exciton dynamics, interface morphologies, charge transfer and transport properties, and so on. For instance, Bao et al. reported a series of OPVs, which adopted the substituted PTCDI polymer as the acceptor and

Received: February 28, 2019
Revised: April 15, 2019
Published: April 15, 2019

DOI: 10.1021/acs.jpca.9b01937
J. Phys. Chem. A 2019, 123, 4034−4047

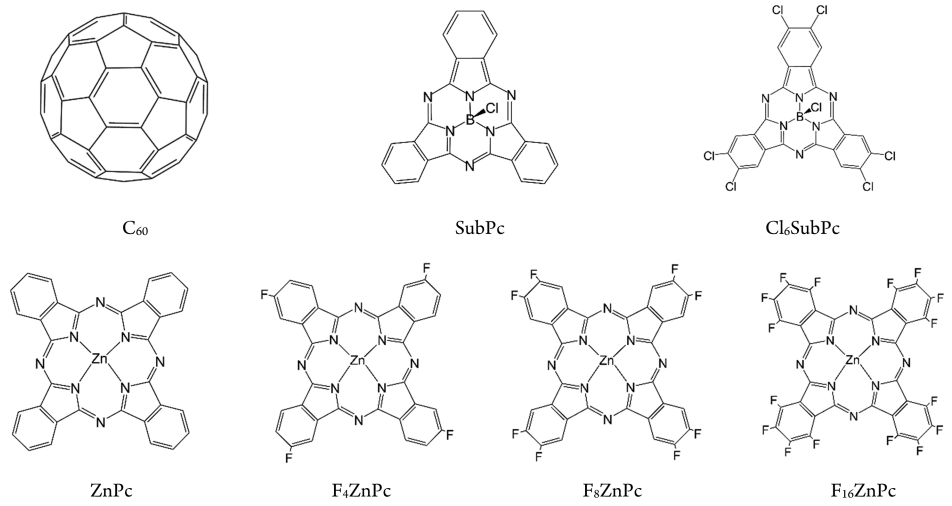

Figure 1. Molecular structures of electron acceptor C_{60} and the electron donors that include boron subphthalocyanine chloride (SubPc), zinc phthalocyanine (ZnPc), and their halogenated derivatives.

polystyrenes with different side chains as donors, that reached PCEs from 1.67 to 4.21%.[8]

Side-chain engineering and backbone repeating-unit modification and substitution are commonly applied strategies of molecular design for electron donor and acceptor materials in OPVs. Among these strategies, halogenation of substituents was demonstrated as an effective method for improving PCE. Experimentally, Ji and co-workers studied the OPVs based on $PC_{71}BM$ as the acceptor and the halogenated (fluorinated, chlorinated, and brominated) small-molecule donors BDTTS-F-R, BDTTSS-Cl-R, and BDTTS-Br-R, reaching PCEs of 9.37, 10.78, and 8.55%, respectively.[9] Zhang et al. investigated the OPVs fabricated using halogenated (fluorinated and chlorinated) small-molecule donors (PBDB-T-2F and PBDB-T-2Cl) and acceptors (IT-4F and IT-4Cl), and the PBDB-T-2Cl/IT-4F heterojunction OPV achieved a PCE up to 14.29%.[10] The PCEs of OPVs based on PBDB-T-2F (fluorinated)/IT-4F and PBDB-T-2Cl(chlorinated)/IT-4F were reported to be as high as 13.2 and 14.4%, respectively,[11] demonstrating that high-performance OPV can be designed by introducing chlorine into the donor's appropriate substituent positions. Chen et al. synthesized a chlorine-substituted new donor PBT4T-Cl, which generated a PCE of 11.18% with the OPV where the active layer constituted of $PC_{71}BM$,[12] and the performance and stability were greatly improved compared to that of the unsubstituted. Liu et al. synthesized another chlorine-substituted donor, coded as J52-2Cl, and the PCE of the OPV combined with the acceptor ITIC reached 11.5%, which was more than three times the unsubstituted donor.[13] Theoretically, Zhao et al. used the Marcus theory to explore the electron transfer properties of model complexes for the $PC_{71}BM$/BTClTT (chlorinated benzothiadiazole connected with two thiophene rings) heterojunction, and the exciton dissociation (ED) and charge recombination (CR) rates were reported to be on the order of $10^{12}-10^{15}$ and $10^{5}-10^{8}$ s^{-1}, respectively.[14] Brédas et al. studied the aggregation on solid-state packing and electronic properties of two donor materials (PBT4T-2OD and PffBT4T-2OD) and found that PffBT4T-2OD after fluorine substitution can maintain planarity during film formation, which is beneficial to maintain a longer interchain interaction and keep stacking order, and then is conducive to exciton dissociation and charge transport.[15] The effectiveness of halogenation was attributed to two aspects. On the one hand, the halogenation of molecules can significantly reduce the molecular orbital energy levels and then increase open circuit voltage.[16,17] On the other hand, the halogenation enhances the inter/intra molecular interaction and improves crystallinity so that the halogenated polymers generally exhibit higher carrier mobility.[18,19]

Metal phthalocyanine and boron subphthalocyanine are important electron donor materials in the fields of OPVs. Schwarze et al. studied the band structures of zinc phthalocyanine and its halogenated derivatives (F_4ZnPc, F_8ZnPc, F_{16}ZnPc) as well as boron subphthalocyanine (SubPc) and its halogenated derivative (Cl_6SubPc) and demonstrated that the optical gap and open circuit voltage can be continuously tuned by the mixing ratio of these donors with C_{60} as the acceptor.[20] The fluorination effects of F_nZnPc (n = 0, 4, 8, 16) on monomer properties and photovoltaic performance of the bilayer OPV with C_{60} was experimentally investigated by Brendel et al.[21] They found that the open circuit voltage increased with the increasing number of F atoms except for F_{16}ZnPc/C_{60}. The fluorination-induced increase of open circuit voltage and PCE was also confirmed by a comparative study of OPV-based F_4ZnPc/C_{60} and ZnPc/C_{60} heterojunctions.[22] The OPV-based SubPc/C_{60} heterojunction was experimentally studied, corresponding to an open circuit voltage of ∼1 eV and PCE of 2.1−3.7%.[23,24] The dependence of charge transfer rates on computational methods and interface geometries was discussed for SubPc/C_{60} and phthalocyanine/C_{60} complexes.[25−28]

The electron processes in the heterojunction interface between donor and acceptor materials of active layers, including charge transfer (CT), ED, CR, and others, can significant impact photocurrent generation in OPVs, which in turn affects the PCE.[29,30] The high CT/ED efficiency and the slow CR rate are expected in order to improve PCE.

However, details of the halogenation effects on electronic structures, photophysical properties, and the kinetics of electron processes in the donor/acceptor heterojunction interface are not systematically studied yet. Hence, in this work, we selected F_nZnPc/C_{60} (n = 0, 4, 8, 16) and Cl_nSubPc/C_{60} (n = 0, 6) as model systems to investigate the halogenation effects of the donor on the electronic structures and excitation

DOI: 10.1021/acs.jpca.9b01937
J. Phys. Chem. A 2019, 123, 4034−4047

properties for donor monomers and donor/C_{60} complexes as well as on the rate constants of CT, ED, and CR for donor/C_{60}. The corresponding molecular structures are given in Figure 1. Because the face-on configuration of the ZnPc/C_{60} heterojunction generated higher open circuit voltage and PCE[31] and the energy of the face-on configuration for the H_2Pc/C_{60} heterojunction is lower than that of the edge-on configuration,[32] the face-on and on-top configurations for F_nZnPc/C_{60} (n = 0, 4, 8, 16) and Cl_nSubPc/C_{60} (n = 0, 6) complexes were constructed as models for heterojunction interfaces, respectively. The other molecular configurations at the interface were not further considered since this work focuses on the halogenation effects rather than the dependence of interface properties on molecular configurations. Density functional theory (DFT) and time-dependent DFT (TDDFT) were applied to study the ground state and excitation properties of donor monomers and donor/C_{60} complexes. The rates of CT, ED, and CR processes were quantitatively explored by using Marcus theory.[33]

2. COMPUTATIONAL METHODS

The ground-state geometrical structures of ZnPc, F_4ZnPc, F_8ZnPc, F_{16}ZnPc, SubPc, Cl_6SubPc, and C_{60} molecules were optimized in the gas phase using density functional theory (DFT) with 6-311G(d,p)[34] basis sets. Due to the existence of non-bond interactions between donor and acceptor molecules in the organic heterojunction, the DFT functional should include dispersion correction. On the other hand, the conventional DFT functional cannot describe the CT nature accurately because of the improper description of long-range asymptotic behavior of $1/r$ (the operator of electron−electron interaction) and many-electron self-interaction error. Hence, the ωB97XD[35] functional was selected in this work since it is a long-range corrected functional including dispersion correction. Then, based on the optimized structures in the gas phase, the geometries in the solid phase were further optimized using the same functional and basis sets. The ZnPc/C_{60}, F_4ZnPc/C_{60}, F_8ZnPc/C_{60}, F_{16}ZnPc/C_{60}, SubPc/C_{60}, and Cl_6SubPc/C_{60} complexes were constructed with the optimized monomers in the solid phase. The solid environment was simulated by using a self-consistent reaction field (SCRF) method with the solute electron density (SMD) model[36] in which the static dielectric constant (ε_s) and the dynamic dielectric constant (ε_d) are required to describe polarization effects of the solid environment. The ε_s and ε_d of ZnPc are 5.0[37] and 2.9,[37,38] respectively, and these values are applied to approximate for the fluorinated derivatives of ZnPc. The ε_s and ε_d of SubPc are 3.9[39] and 2.1,[40] respectively, and the same values were applied for the chlorinated derivative Cl_6SubPc. For C_{60}, the ε_s is 5.0,[41] and the ε_d is 3.3 where the ε_d (3.3) is approximated as the square of the C_{60} refractive index 1.813.[42,43] Considering the long-range isotropic polarization effect in the organic photovoltaic bulk heterojunction, the ε_s and ε_d of the monomers and complexes in the solid phase were adopted as the average values of the corresponding electron donors and C_{60}.

Compared to experimental results, the long-range corrected hybrid functionals in DFT with optimally tuned range-separation parameter ω were successful in the excited-state calculations. Based upon Koopmans' theorem and the quantum chemistry calculation of the monomers in the solid phase combined with the reported methods,[44,45] the following equation was used to optimize ω

$$
\begin{aligned}
J_1(\omega) &= |\varepsilon_{D(HOMO)}(\omega) + E_D^+(\omega) - E_D(\omega)\cdot \\
&\quad + |\varepsilon_{A(HOMO)}(\omega) + E_A^+(\omega) - E_A(\omega)| \\
J_2(\omega) &= |\varepsilon_{D(HOMO)}(\omega) + E_D^+(\omega) - E_D(\omega)| \\
&\quad + |\varepsilon_{A(HOMO)}^-(\omega) + E_A(\omega) - E_A^-(\omega)| \\
J(\omega) &= J_1(\omega) + J_2(\omega)
\end{aligned} \tag{1}
$$

where subscripts D and A represent donors and acceptors, respectively, $\varepsilon_{(HOMO)}(\omega)$ is the highest occupied molecular orbital (HOMO) energy of the neutral state at the given ω, and $\varepsilon_{A(HOMO)}^-(\omega)$ is the HOMO energy of the acceptor anionic state; $E(\omega)$ is the energy of the neutral state of the D (A) at the given ω and $E^+(\omega)$ and $E^-(\omega)$ are the single-point energies of the cationic state and the anionic state, respectively. $J_1(\omega)$ minimum represents the ionization potential (IP) optimization of ω for the donor and acceptor, which can give a good description of the local excitation, while $J_2(\omega)$ minimum corresponds to the IP tuning of ω for the donor and the electronic affinity potential tuning (EA tuning) of ω for the acceptor, which can describe charge transfer excitation well. Due to the existence of local and CT excitations in donor/C_{60} complexes, the optimally tuned ω using $J(\omega)$ minimum must be suitable for the calculations of both local and CT excitations. The optimally tuned ω values are 0.002, 0.002, 0.001, 0.001, 0.004, and 0.004 $Bohr^{-1}$ for ZnPc/C_{60}, F_{16}ZnPc/C_{60}, F_4ZnPc/C_{60}, F_8ZnPc/C_{60}, SubPc/C_{60}, and Cl_6SubPc/C_{60} complexes, respectively. The geometries of complexes in the solid phase were fully optimized using ωB97XD/6-311G(d,p) with the optimally tuned ω. The excitation properties of the monomers and the complexes in the solid phase were calculated using TDDFT methods at the level of ωB97XD/6-311G(d,p) with the optimally tuned ω. We also applied the optimally tuned ω in the calculations of excitation, reorganization energies, free energy changes, and electron coupling.

The quantum chemistry calculations based upon DFT and TDDFT were performed by using the Gaussian 09 package.[46] In addition, in order to characterize the excitation characters, Multiwfn was adopted to calculate the charge density difference (CDD) map, charge transfer distance, and the transferred charges of the complexes.[47,48]

The kinetics of electron processes CT, ED, and CR can be characterized using rate constants. The photoinduced direct CT process is DA → D^+A^-, the ED is D*A → D^+A^- (D*A is the exciton state localized in the donor, and the D^+ and A^- ions in the final state correspond to the CT state), and the CR process is D^+A^- → DA. The comparison of rate constants calculated using Marcus theory, Fermi's golden rule, and the second-order cumulant expansion of the time-dependent reduced density matrix pointed out that Marcus theory can provide qualitatively correct values of rates.[49] Hence, considering the motivation of this work, we applied Marcus theory to investigate the donor halogenation effects on electron processes rates of the donor/C_{60} heterojunction interface. In terms of Marcus theory,[33] the rate constants of CT, ED, and CR processes at room temperature (T = 300 K) were calculated with the following formula

$$
k = \sqrt{\frac{4\pi^3}{h^2 \lambda k_B T}}\, |V_{DA}|^2 \exp\left(-\frac{(\Delta G + \lambda)^2}{4\lambda k_B T}\right) \tag{2}
$$

DOI: 10.1021/acs.jpca.9b01937
J. Phys. Chem. A 2019, 123, 4034−4047

Table 1. Lowest Singlet Excitation Energy E_{S1}(eV), HOMO Level (eV), LUMO Level (eV), HOMO−LUMO Gap ($H-L_{gap}$, eV), Energy Difference ΔE_{T-S} (eV) between the Singlet Ground State S0 and the Triplet State T1 for the Monomers Calculated at the Given ω Value (in $Bohr^{-1}$), and Static ε_s and Dynamic ε_d Dielectric Constants

molecule	ω, ε_s, ε_d	E_{S1}	HOMO	LUMO	$H-L_{gap}$	ΔE_{T-S}
ZnPc	0.002, 5, 3.1	1.9650	−4.9745	−2.6343	2.3402	1.228
F_4ZnPc	0.001, 5, 3.1	1.9767	−5.1117	−2.7870	2.3247	1.221
F_8ZnPc	0.001, 5, 3.1	2.0010	−5.2570	−2.9073	2.3497	1.237
F_{16}ZnPc	0.002, 5, 3.1	1.9179	−5.4752	−3.1973	2.2779	1.213
SubPc	0.004, 4.45, 2.7	2.4082	−5.3593	−2.4368	2.9225	1.601
Cl_6SubPc	0.004, 4.45, 2.7	2.3784	−5.7307	−2.8368	2.8939	1.600

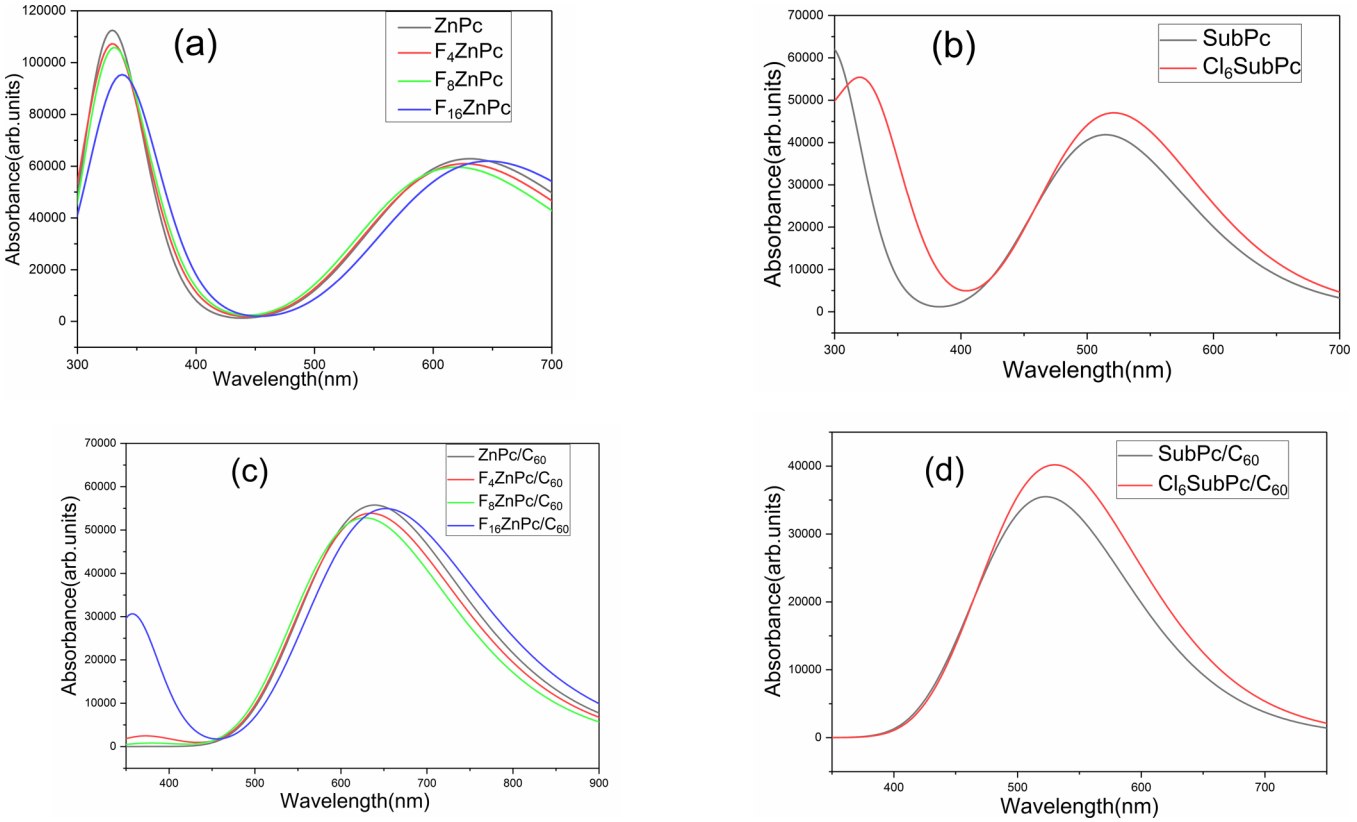

Figure 2. Simulated absorption spectra of (a, b) the monomers and (c, d) complexes.

where λ is the reorganization energy, V_{DA} is the electron coupling between the initial and final states, k_B is the Boltzmann constant, h is Planck's constant, and ΔG is the free energy change. The computational details of λ, V_{DA}, ΔG, and rate constants were reported in our previous work.[50] The degeneracy of electronic donor and acceptor C_{60} was considered during the calculations of effective electronic coupling.

3. RESULTS AND DISCUSSION

3.1. F_nZnPc (n = 0, 4, 8, 16) and Cl_nSubPc (n = 0, 6) Properties. The molecular structures of the monomers and complexes with the selected atomic serial numbers for labeling geometrical parameters are given in Figure S1 in the Supporting Information. The selected bond lengths (in Å) and bond angles and dihedral angles (in °) of the optimized F_nZnPc (n = 0, 4, 8, 16) and Cl_nSubPc (n = 0, 6) molecules are listed in Table S1 in the Supporting Information. The dihedral angles of the optimized F_nZnPc (n = 0, 4, 8, 16) molecules agree with their planar structures, which can facilitate electron delocalization. The averaged C−F bond lengths are 1.347, 1.338, and 1.328 Å for F_4ZnPc, F_8ZnPc, and F_{16}ZnPc, respectively. The reduction of C−F bond lengths indicates the enhancement of C−F bonds with the increasing number of F atoms in F_nZnPc (n = 0, 4, 8, 16) molecules. Due to the local character of chemical bonds, the other geometrical parameters (bond lengths, bond angles, and dihedral angles; see Table S1 in the Supporting Information) are quite similar for F_nZnPc (n = 0, 4, 8, 16) molecules. The optimized structures of Cl_nSubPc (n = 0, 6) molecules are like an inverted umbrella.

The B−Cl bond lengths are 1.881 and 1.872 Å for SubPc and Cl_6SubPc, respectively. The averaged Cl−C bond length is 1.739 Å for Cl_6SubPc. The other geometrical parameters of SubPc and Cl_6SubPc are almost the same.

The molecular HOMO and LUMO energies can be applied to characterize redox properties. The HOMO, LUMO, and HOMO−LUMO gap for F_nZnPc (n = 0, 4, 8, 16) and Cl_nSubPc (n = 0, 6) molecules are listed in Table 1. For F_nZnPc (n = 0, 4, 8, 16), with the increasing number of F atoms, the HOMO and LUMO are stabilized because of strong F−C bonds. The HOMO−LUMO gap of F_nZnPc (n = 0, 4, 8,

DOI: 10.1021/acs.jpca.9b01937
J. Phys. Chem. A 2019, 123, 4034−4047

Table 2. Electronic Transition Energies (eV), Excitation Wavelengths (nm), Corresponding Oscillator Strengths (f), and Main Transition Configurations for F_nZnPc (n = 0, 4, 8, 16) and Cl_nSubPc (n = 0, 6) Molecules

molecule	states	main transition configurations	E (eV/nm)	f
ZnPc	S1	H → L (97.40%)	1.9650/630.97	0.7762
	S2	H → L + 1 (97.40%)	1.9650/630.97	0.7761
	S15	H − 6 → L (69.97%); H − 5 → L (18.49%)	3.7456/331.01	0.1826
	S16	H − 6 → L + 1 (69.98%); H − 5 → L + 1 (18.48%)	3.7456/331.01	0.1825
	S17	H − 5 → L (58.26%); H − 9 → L + 1 (24.67%)	3.7658/329.24	1.1458
	S18	H − 5 → L + 1 (58.26%); H − 9 → L (24.67%)	3.7658/329.24	1.1458
F_4ZnPc	S1	H → L (97.30%)	1.9767/627.22	0.7540
	S2	H → L + 1 (97.30%)	1.9768/627.21	0.7540
	S14	H − 5 → L (70.52%); H − 6 → L (18.77%)	3.6242/342.10	0.2820
	S15	H − 5 → L + 1 (70.52%); H − 6 → L + 1 (18.78%)	3.6242/342.10	0.2819
	S17	H − 6 → L (56.89%); H − 5 → L (20.03%)	3.7869/327.40	1.0377
	S18	H − 6 → L + 1 (56.89%); H − 5 → L + 1 (20.03%)	3.7869/327.40	1.0377
F_8ZnPc	S1	H → L (95.65%)	2.0010/619.60	0.7361
	S2	H → L + 1 (95.65%)	2.0010/619.60	0.7361
	S11	H − 4 → L (83.01%)	3.5243/351.80	0.3061
	S12	H − 4 → L + 1 (83.01%)	3.5243/351.80	0.3062
	S17	H − 6 → L (66.97%)	3.7832/327.72	1.0386
	S18	H − 6 → L + 1 (66.97%)	3.7832/327.72	1.0386
F_{16}ZnPc	S1	H → L (96.47%)	1.9179/646.45	0.7648
	S2	H → L + 1 (96.47%)	1.9179/646.45	0.7648
	S13	H − 3 → L (82.76%)	3.4981/354.43	0.3889
	S14	H − 3 → L + 1 (82.76%)	3.4981/354.43	0.3889
	S20	H − 8 → L (42.72%); H − 9 → L (47.55%)	3.6995/335.14	0.4072
	S21	H − 9 → L + 1 (47.55%); H − 8 → L + 1 (42.73%)	3.6995/335.14	0.4072
	S22	H − 8 → L (39.55%); H − 9 → L (26.64%); H − 11 → L + 1 (13.79%)	3.7251/332.84	0.4081
	S23	H − 8 → L + 1 (39.55%); H − 9 → L + 1 (26.64%); H − 11 → L (13.79%)	3.7251/332.84	0.4081
SubPc	S1	H → L (97.61%)	2.4082/514.84	0.5166
	S2	H → L + 1 (97.59%)	2.4104/514.38	0.5166
	S10	H − 3 → L (86.79%)	4.0957/302.72	0.4263
	S11	H − 3 → L + 1 (86.69%)	4.0978/302.56	0.4274
Cl_6SubPc	S1	H → L (97.33%)	2.3784/521.30	0.5806
	S2	H → L + 1 (97.32%)	2.3795/521.04	0.5803
	S7	H − 3 → L (88.16%)	3.7461/330.97	0.4820
	S8	H − 3 → L + 1 (87.89%)	3.7467/330.92	0.4839

16) molecules, ranging from2.28 (F_{16}ZnPc) to 2.35 eV (F_8ZnPc), does not monotonically depend on the extent of fluorination. Furthermore, the experimental HOMO and LUMO offsets of F_nZnPc (n = 0, 4, 8, 16) with respect to C_{60}[21] were well reproduced by this work. For Cl_nSubPc (n = 0, 6), the chlorination stabilizes the HOMO and LUMO by ∼0.37 and 0.40 eV, respectively, generating a slight reduction of the HOMO−LUMO gap (∼0.03 eV). This agrees well with experimental results (lowering of HOMO and LUMO by at least 0.3 eV), which were obtained using cyclic voltammetry and ultraviolet electronic absorption spectroscopy.[51] The stabilization of the HOMO and LUMO induced by fluorination and chlorination for F_nZnPc (n = 0, 4, 8, 16) and Cl_nSubPc (n = 0, 6) corresponds to the increase of IP and EA.

To explore the excitation properties, 30 and 15 singlet excited states were calculated for F_nZnPc (n = 0, 4, 8, 16) and Cl_nSubPc (n = 0, 6), respectively. The lowest singlet excitation energy E_{S1} and the energy difference ΔE_{T-S} between the ground state S0 and the triplet state T1 for F_nZnPc (n = 0, 4, 8, 16) and Cl_nSubPc (n = 0, 6) molecules are summarized in Table 1. The ΔE_{T-S} values, which were calculated using the ΔSCF method based on the optimized ground state, can approximate the lowest triplet vertical excitation energy. The ranges of E_{S1} and ΔE_{T-S} for F_nZnPc (n = 0, 4, 8, 16) are 1.918−2.001 eV and 1.213−1.237 eV, respectively. Among F_nZnPc (n = 0, 4, 8, 16), F_8ZnPc has the largest excitation energies E_{S1} and ΔE_{T-S}, whereas F_{16}ZnPc has the smallest E_{S1} and ΔE_{T-S} because of its HOMO−LUMO gap. As for Cl_nSubPc (n = 0, 6), it can be found that introducing Cl reduces E_{S1} and ΔE_{T-S} by ∼0.03 and <0.01 eV, respectively. Hence, the impact of halogenation on excitation energies (E_{S1} and ΔE_{T-S}) for F_nZnPc (n = 0, 4, 8, 16) and Cl_nSubPc (n = 0, 6) molecules is not remarkable as that on MO energies.

It was observed that the absorption profiles of F_nZnPc (n = 0,4,8) were very similar, while the absorption peaks of F_{16}ZnPc exhibited a tiny red shift, and the B-band absorption maximum of the F_nZnPc film was ∼3.65 eV, whereas the Q band was split into two peaks at ∼1.72−1.79 and 1.89−2.00 eV.[21] The simulated absorption spectra are presented in Figure 2. The excitation energy ranges of F_nZnPc (n = 0,4,8) are 1.918−2.001 and 3.700−3.787 eV for the Q and B bands, respectively. Except the splitting of the Q band (the reasons will be described in the next paragraph), both the absorption profiles and maxima of experimental spectra were well reproduced by the simulated spectra. For example, the calculated absorption maxima of the F_{16}ZnPc Q band (1.91 eV) agree well with those of the experimental result (1.89 eV).[21] The absorption

DOI: 10.1021/acs.jpca.9b01937
J. Phys. Chem. A 2019, 123, 4034−4047

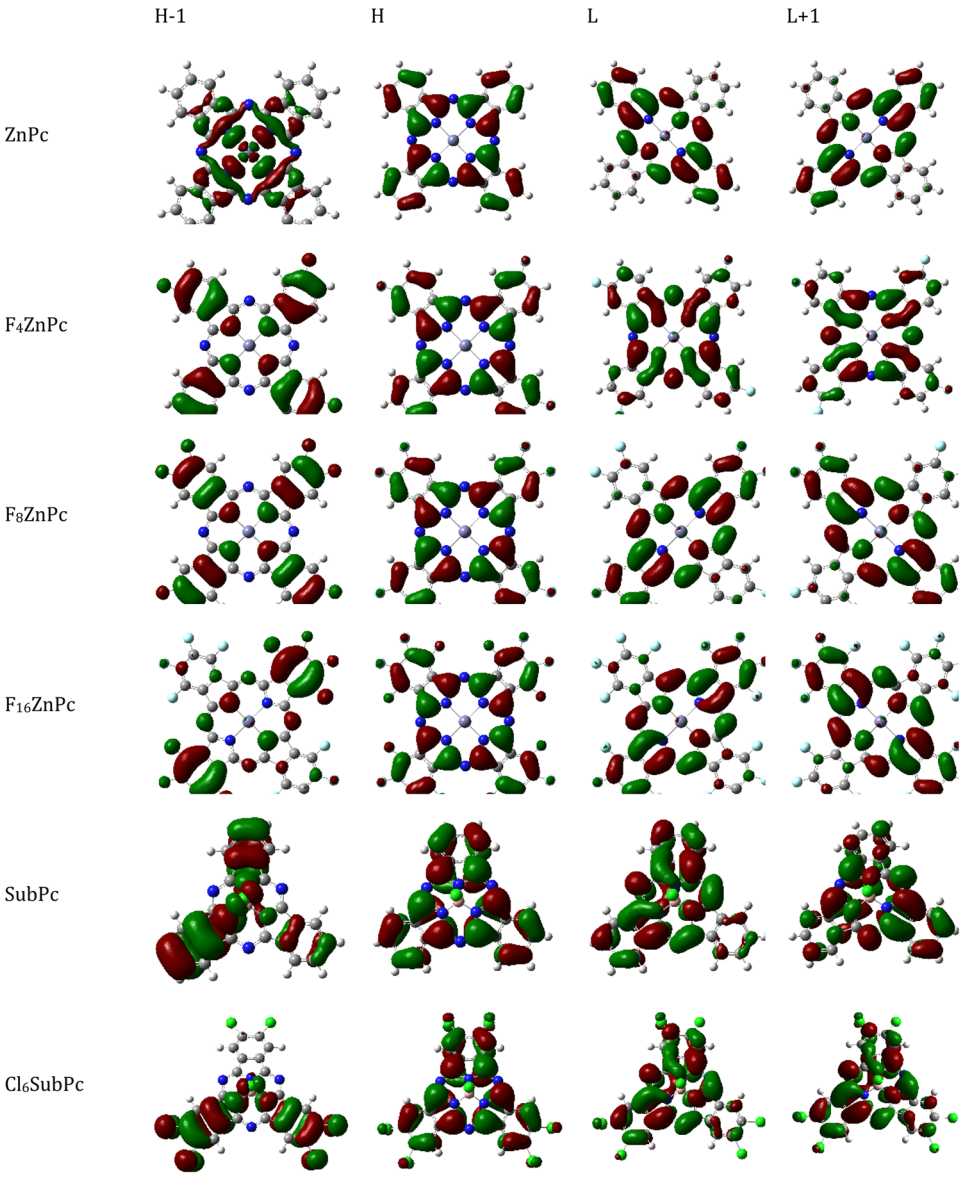

Figure 3. Selected frontier molecular orbitals for the ZnPc, F4ZnPc, F8ZnPc, F16ZnPc, SubPc, and Cl_6SubPc (H = HOMO, L = LUMO, ωB97XD/ 6-311G(d,p)).

profile of Cl_6SubPc is similar to that of SubPc.[52] The SubPc film was observed to have two absorption peaks at ∼580 nm (2.12 eV) and 300 nm (4.08 eV).[53] These are close to the two absorption peaks of the Q band at 515 nm (2.41 eV) and the B band at 303 nm (4.10 eV), which we calculated in the solid phase. In terms of the absorption spectra of F_nZnPc (n = 0, 4, 8, 16) and Cl_nSubPc (n = 0, 6), the halogenated effects can be found, that is, the absorption spectra of F_{16}ZnPc exhibit a red shift relative to those of other F_nZnPc (n = 0, 4, 8) molecules, and the absorption spectra of Cl_nSubPc (n = 0, 6) support the fact that the chlorination induced a red shift of absorption bands in the visible region. The red shift of absorption spectra is expected because it may enhance the light-harvesting abilities.

Table 2 lists the electronic transition energies, excitation wavelengths (λ > 300 nm), and the corresponding oscillator strengths (f > 0.1) as well as the main transition configurations. The selected molecular orbitals (MOs) are presented in Figure 3. More detailed data and MOs for excited states are given in Table S2 and Figures S2 and S3 in the Supporting Information, respectively. Most of the excited states of F_nZnPc (n = 0, 4, 8) exhibit doublet degeneracy due to their symmetry. Similarly, most of the excited states of Cl_nSubPc (n = 0, 6) also have doublet quasi-degeneracy. Intermolecular interactions of molecular packing in the solid phase can break the molecular symmetry, leading to elimination of symmetry and splitting of the Q band. Furthermore, the frontier MOs (see Figure 3 and Figures S2 and S3) of F_nZnPc (n = 4, 8, 16) and Cl_6SubPc indicate that the introduced F and Cl atoms have different extents of contribution, meaning the effectiveness of fluorination and chlorination for tuning excitation properties because the introduced F and Cl atoms take part in excitation. Meanwhile, it should be noticed that for F_nZnPc (n = 0, 8, 16) and Cl_6SubPc, the relocation of MOs involved in transition suggests that the excited states show a CT character, for instance, the S1 and S2 excited states of F_nZnPc (n = 0, 8, 16). Relative to local excitation, the intramolecular CT excitation

DOI: 10.1021/acs.jpca.9b01937
J. Phys. Chem. A 2019, 123, 4034−4047

Table 3. HOMO Energies (eV), LUMO Energies (eV), HOMO−LUMO Gaps (H−L_{gap}, in eV), Lowest Singlet Excitation Energies E_{S1} (eV), Geometric Center Distances D_{D-A} (Å) between Donor and Acceptor of the Complexes, and Binding Energies E_b (eV) of the Complexes Formed by Donor and Acceptor

complex	HOMO	LUMO	H−L_{gap}	E_{S1}	D_{D-A}	E_b
ZnPc/C_{60}	−4.9751	−3.2148	1.7603	1.3571	8.26	0.3828
F_4ZnPc/C_{60}	−5.1225	−3.2556	1.8670	1.4822	8.13	0.3941
F_8ZnPc/C_{60}	−5.2812	−3.2746	2.0066	1.6245	8.25	0.4029
F_{16}ZnPc/C_{60}	−5.5182	−3.2969	2.2213	1.8174	8.20	0.4505
SubPc/C_{60}	−5.3620	−3.2270	2.1350	1.6767	7.93	0.3061
Cl_6SubPc/C_{60}	−5.7424	−3.2425	2.4999	2.0361	7.85	0.3567

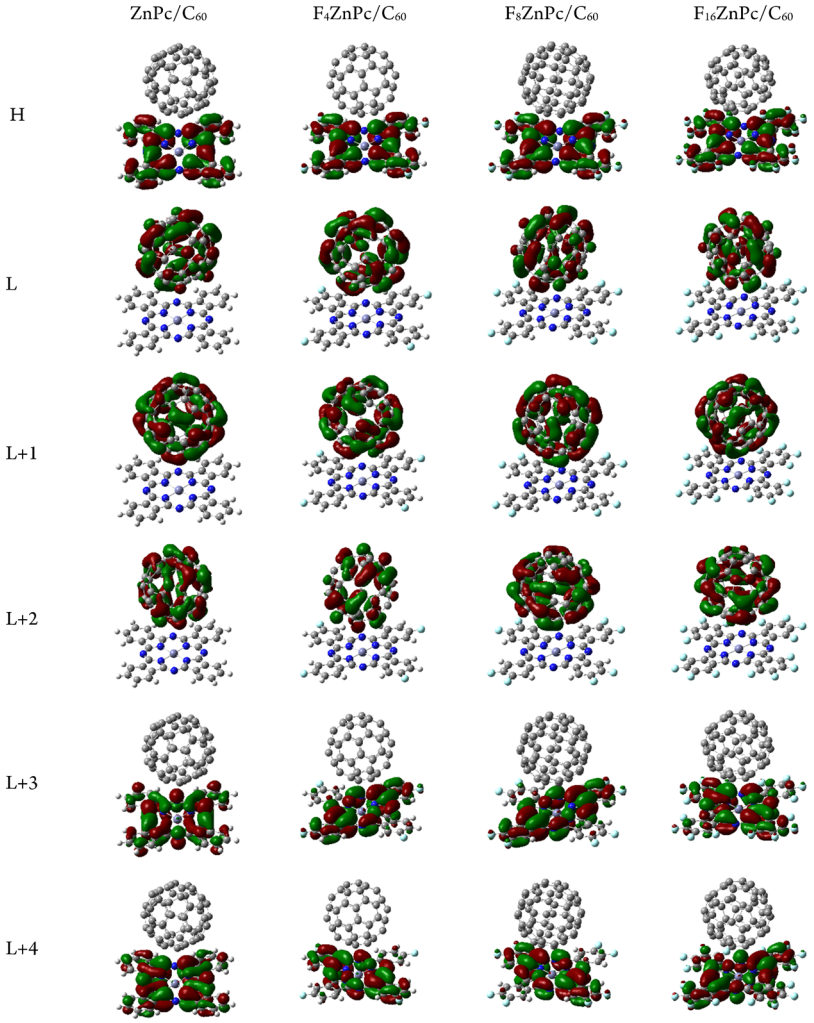

Figure 4. Selected frontier molecular orbitals for the ZnPc/C_{60}, F_4ZnPc/C_{60}, F_8ZnPc/C_{60}, and F_{16}ZnPc/C_{60} complexes (H = HOMO, L = LUMO, ωB97XD/ 6-311G(d,p)).

can reduce the exciton binding energy,[S4] which is the energy barrier for the separation of the attracted electron−hole pairs. Thus, the intramolecular CT is advantageous to F_nZnPc (n = 0, 8,16) and Cl_6SubPc for their ED process.

3.2. F_nZnPc/C_{60} (n = 0, 4, 8, 16) and Cl_nSubPc/C_{60} (n = 0, 6) Properties. The optimized geometries for face-on ZnPc/C_{60} and on-top SubPc/C_{60} complexes are presented in Figure S1 in the Supporting Information. The optimized geometries for face-on F_nZnPc/C_{60} (n = 4, 8, 16) and on-top Cl_6SubPc/C_{60} complexes are similar to those of ZnPc/C_{60} and SubPc/C_{60}, respectively. The selected geometric parameters are given in Table S3 in the Supporting Information. The comparison of corresponding geometric parameters in monomers and the complexes indicates that due to the weak intermolecular interaction between the donor and C_{60}, the corresponding bond lengths are almost unchanged and the variations of the corresponding the bond angles and the dihedral angles are smaller than 1°. Hence, F_nZnPc (n = 0, 4, 8, 16) samples maintain a quasi-planar structure in the complexes, and Cl_nSubPc (n = 0, 6) samples retain their inverted umbrella structures. The distances between the C_{60} center and the Zn atom in F_nZnPc (n = 0, 4, 8, 16) range from 8.13 to 8.26 Å, and the distances between the C_{60} center and the center of Cl_nSubPc (n = 0, 6) are about 7.85∼7.93 Å. Generally, the halogenation induces the shorter intermolecular distance in these complexes. However, the distances between

DOI: 10.1021/acs.jpca.9b01937
J. Phys. Chem. A 2019, 123, 4034−4047

the C_{60} center and the Zn atom in F_nZnPc (n = 0, 4, 8, 16) do not monotonically depend on the extent of fluorination. These distances are longer than the molecular center distance between pentacene and C_{60} in pentacene/C_{60} complexes with a face-on configuration.[55] The longer D−A distance in complexes lead to a reduction of effective electronic coupling.[56]

The binding energies E_b, which were calculated as the total energy differences between the complexes and the corresponding monomers, are about 0.4 eV (see Table 3) where the binding energy of ZnPc/C_{60} of 0.38 eV is consistent with the theoretically calculated value of 0.37 eV for CuPc/C_{60}.[57] The data of E_b also indicate that the halogenation enhances the non-bond interaction between the donor and C_{60} in these complexes, and this tendency is in line with halogenation effects on intermolecular distance in complexes. Furthermore, E_b increases with increasing extent of fluorination in F_nZnPc (n = 0, 4, 8, 16). It is interesting that the order of E_b for F_nZnPc/C_{60} (n = 0, 4, 8, 16) complexes is consistent with that of absolute values of the main component of an electric quadrupole tensor (xx, yy, and zz components, the quantities are listed in Table S4 in the Supporting Information) for F_nZnPc (n = 0, 4, 8, 16). It is the same for Cl_nSubPc/C_{60} (n = 0, 6) complexes. Considering the symmetry of C_{60}, F_nZnPc (n = 0, 4, 8, 16), and Cl_nSubPc/C_{60} (n = 0, 6), the non-bond interaction between donor and C_{60} might be mainly determined by their electric quadrupole moment.

Table 3 also lists the HOMO and LUMO energies as well as HOMO−LUMO gaps of F_nZnPc/C_{60} (n = 0, 4, 8, 16) and Cl_nSubPc/C_{60} (n = 0, 6) complexes. Because the LUMOs of complexes are localized in C_{60} and the HOMOs are mainly contributed by donors (see Figures 4 and 5), the fluorination of ZnPc and the chlorination of SubPc generate remarkable stabilization of the HOMO and a slight decrease of the LUMO for complexes, resulting in a broadening of the HOMO−LUMO gaps (from 1.76 to 2.22 eV for F_nZnPc (n = 0, 4, 8, 16) and from 2.14 to 2.50 eV for Cl_nSubPc (n = 0, 6)). Certainly, due to the weak non-bond interaction between the donor and C_{60} in complexes, the HOMO variations of F_nZnPc/C_{60} (n = 0, 4, 8, 16) and Cl_nSubPc/C_{60} (n = 0, 6) complexes are quite tiny relative to the HOMOs of F_nZnPc (n = 0, 4, 8, 16) and Cl_nSubPc (n = 0, 6).

The simulated absorption spectra of F_nZnPc/C_{60} (n = 0, 4, 8, 16) and Cl_nSubPc/C_{60} (n = 0, 6) complexes are also presented in Figure 2. Compared with the monomer absorption spectra, the complexes' absorption bands in the visible region exhibit a red shift by ∼8 nm. The halogenation effects on the complexes' absorption spectra are very similar to the monomers'. The λ_{max} at absorption maximum for F_nZnPc/C_{60} (n = 0, 4) agrees well with that of experimental external quantum efficiency spectra for F_nZnPc(30 nm)/C_{60}(35 nm) bilayer solar cells.[21]

The lowest singlet excitation energies E_{S1} of F_nZnPc/C_{60} (n = 0, 4, 8, 16) and Cl_nSubPc/C_{60} (n = 0, 6) complexes are collected in Table 3 in order to clearly expose halogenation effects. The fluorination of ZnPc and the chlorination of SubPc increase the E_{S1} of complexes. This is similar to that of chlorinated benzothiadiazole-based polymers as donors and $PC_{71}BM$ as the acceptor.[14] The HOMO−LUMO gap order of F_nZnPc/C_{60} (n = 0, 4, 8, 16) and Cl_nSubPc/C_{60} (n = 0, 6) complexes are the same as the order of the lowest singlet excitation energies E_{S1}, meaning the simple transition configuration of the S1 exited state.

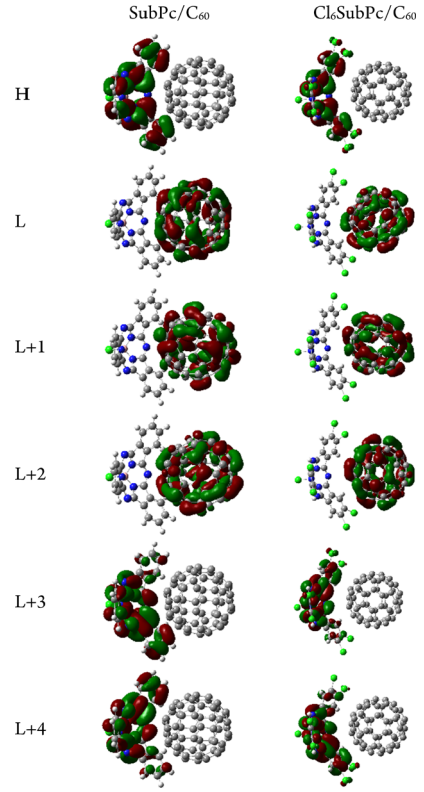

Figure 5. Selected frontier molecular orbitals for the SubPc/C_{60} and Cl_6SubPc/ C_{60} complexes (H = HOMO, L = LUMO, ωB97XD/ 6-311G(d,p)).

To understand the details of excited states, the main transition configurations, the excitation energies, wavelengths, and oscillator strengths of F_nZnPc/C_{60} (n = 0, 4, 8, 16) and Cl_nSubPc/C_{60} (n = 0, 6) complexes are listed in Table 4 for the selected excited states, including CT excited states and local excited states in the donor. The related MOs are presented in Figures 4 and 5. The details of more excited states and MOs are listed in Tables S5 and S6 and Figures S4 and S5 in the Supporting Information. It can be found that the excitation energy differences for many excited states are very small, suggesting quasi-degenerate excitations, which resulted from symmetry of the donor and acceptor. The HOMO, LUMO + 3, and LUMO + 4 of F_nZnPc/C_{60} (n = 0, 4, 8, 16) and Cl_nSubPc/C_{60} (n = 0, 6) complexes are mainly contributed by electron donor moieties, while the other MOs are localized in C_{60}. Hence, the S1−S3 of F_nZnPc/C_{60} (n = 0, 4, 8, 16) complexes are quasi-degenerate "dark" CT states, S4 and S5 are quasi-degenerate "bright" local excited states in donor moieties, S6−S20 are local excited states in C_{60}, and S31−S33 are quasi-degenerate CT states with higher energies. The MO characters determine the similar excitation properties of F_nZnPc/C_{60} (n = 0, 4, 8, 16) complexes. The excitation properties of Cl_nSubPc/C_{60} (n = 0, 6) complexes are also similar. The S1−S3 of Cl_nSubPc/C_{60} (n = 0, 6) complexes are quasi-degenerate CT states, S19 and S20 are quasi-degenerate local excited states in donor moieties, and S4−S18 are local excited states in C_{60}. From an energetic view, the higher energy of local excited states of electron donor permits it to decay to CT states at the donor−acceptor interface. The excitation characters (CT and local excitations) for the selected excitations can be further confirmed by the charge density

DOI: 10.1021/acs.jpca.9b01937
J. Phys. Chem. A 2019, 123, 4034−4047

Table 4. Excitation Energies (Wavelengths), Corresponding Oscillator Strengths (f), Excited State Characters (ESC), and Main Transition Configurations of the F_nZnPc/C_{60} (n = 0, 4, 8, 16) and Cl_nSubPc/C_{60} (n = 0, 6) Complexes

complex	states	main transition configurations	ESC	E (eV/nm)	f
$ZnPc/C_{60}$	S1	H → L (90.08%)	CT	1.3571/913.61	0.0000
	S2	H → L + 2 (95.30%)	CT	1.3600/911.63	0.0000
	S3	H → L + 1 (86.66%)	CT	1.3726/903.29	0.0000
	S4	H → L + 3 (95.30%)	DLE	1.9388/639.48	0.6872
	S5	H → L + 4 (95.28%)	DLE	1.9402/639.03	0.6895
F_4ZnPc/C_{60}	S1	H → L (99.53%)	CT	1.4822/836.48	0.0000
	S2	H → L + 2 (79.36%); H → L + 1 (20.31%)	CT	1.4848/835.02	0.0000
	S3	H → L + 1 (79.46%); H → L + 2 (20.37%)	CT	1.4994/826.92	0.0000
	S4	H → L + 3 (96.88%)	DLE	1.9522/635.09	0.6669
	S5	H → L + 4 (96.84%)	DLE	1.9546/634.31	0.6629
F_8ZnPc/C_{60}	S1	H → L (99.28%)	CT	1.6245/763.19	0.0001
	S2	H → L + 1 (95.58%)	CT	1.6284/761.39	0.0000
	S3	H → L + 2 (95.46%)	CT	1.6453/753.56	0.0000
	S4	H → L + 3 (96.89%)	DLE	1.9740/628.10	0.6516
	S5	H → L + 4 (96.87%)	DLE	1.9751/627.72	0.6521
$F_{16}ZnPc/C_{60}$	S1	H → L (98.81%)	CT	1.8174/682.21	0.0018
	S2	H → L + 1 (99.07%)	CT	1.8202/681.17	0.0002
	S3	H → L + 2 (99.55%)	CT	1.8417/673.22	0.0001
	S4	H → L + 3 (96.40%)	DLE	1.9008/652.26	0.6784
	S5	H → L + 4 (96.59%)	DLE	1.9012/652.14	0.6763
$SubPc/C_{60}$	S1	H → L + 1 (96.90%)	CT	1.6767/739.44	0.0000
	S2	H → L + 2 (95.92%)	CT	1.6779/738.92	0.0000
	S3	H → L (97.58%)	CT	1.6896/733.81	0.0000
	S19	H → L + 3 (96.18%)	DLE	2.3714/522.84	0.4311
	S20	H → L + 4 (96.02%)	DLE	2.3735/522.37	0.4316
Cl_6SubPc/C_{60}	S1	H → L (91.39%)	CT	2.0361/608.92	0.0000
	S2	H → L + 1 (92.29%)	CT	2.0377/608.45	0.0000
	S3	H → L + 2 (95.97%)	CT	2.0565/602.88	0.0000
	S19	H → L + 3 (91.58%)	DLE	2.3402/529.81	0.4736
	S20	H → L + 4 (91.64%)	DLE	2.3423/529.32	0.4723

difference, which are presented in Figures 6 and 7 for F_nZnPc/C_{60} (n = 0, 4, 8, 16) and Cl_nSubPc/C_{60} (n = 0, 6) complexes, respectively.

To get a quantitative description of CT and local excitations, the transferred charges (Δq) and CT distances (Δd) (marked in Figures 6 and 7) of F_nZnPc/C_{60} (n = 0, 4, 8, 16) and Cl_nSubPc/C_{60} (n = 0, 6) complexes were calculated. The CT distances of S1−S3 states are very close to the distances between molecular centers. The transferred charges of S1−S3 states are almost unity, meaning the integer electron transfer, whereas the small transferred charges (<0.05 e) and CT distances for S4 and S5 for F_nZnPc/C_{60} (n = 0, 4, 8, 16) complexes and S19 and S20 for Cl_nSubPc/C_{60} (n = 0, 6) complexes provide confirmation of the local excitation in donor moieties. In addition, the charge transfer distances of these three states are ∼8.1−8.3 Å, which are very close to the geometric center distance of the donor and C_{60}.

Compared with the experimental CT excitation energy of $F_5BsubPc/C_{60}$ complexes (∼1.7 eV),[58] the calculated CT energies (see Table 4) of Cl_nSubPc/C_{60} (n = 0, 6) complexes are reasonable. Meanwhile, in terms of the empirical relationship between CT excitation energy and open-circuit voltage V_{OC}[27]

$$qV_{OC} = E(CT_1) - (0.6 \pm 0.1)\ \text{eV} \quad (3)$$

the higher CT excitation energies are favorable for increasing V_{OC}. The V_{OC} deduced from CT excitation energy agrees well with that of experimental results, meaning the reliability of calculated CT excitation energies. For instance, the CT energy of $SubPc/C_{60}$ complexes (1.68 eV) generates a V_{OC} of ∼1.08±0.1 eV, agreeing well with the experimental V_{OC} (1.10 eV).[51] The data in Table 4 indicate that fluorination of ZnPc and chlorination of SubPc increase the CT excitation energies of F_nZnPc/C_{60} (n = 0, 4, 8, 16) and Cl_nSubPc/C_{60} (n = 0, 6) complexes. Hence, the fluorination of ZnPc and chlorination of SubPc can improve the V_{OC} for F_nZnPc/C_{60} (n = 0, 4, 8, 16) and Cl_nSubPc/C_{60} (n = 0, 6) heterojunctions because of the halogenation effects on CT excitation energies. In the experiment, the V_{OC} of F_nZnPc/C_{60} (n = 0, 4, 8) is also increased, but $F_{16}ZnPc/C_{60}$ is decreased.[21] Due to the limitations of the empirical eq 3, the theoretically calculated uptrend results for $F_{16}ZnPc/C_{60}$ do not match the experimental decline. This doubt can be understood from the ED rate discussed in Section 3.3.

3.3. Rate Constants of Charge Transfer, Exciton Dissociation, and Charge Recombination. The parameters required for calculating ΔG are given in Table 5, and the calculated ΔG values for CT, ED, and CR processes are listed in Table 6. It should be noted that for photoinduced direct CT processes, the incident photon energy must be absorbed, corresponding to the DA + $h\gamma \rightarrow D^+A^-$ process, and the ΔG between the initial and final states should be taken into account for photon energy. The ΔG values listed in Table 6 indicate that for F_nZnPc/C_{60} (n = 4, 8, 16) and $SubPc/C_{60}$ (n = 0, 6) complexes, $|\Delta G|$ is reduced with increasing halogenation degree during the CT process. The $|\Delta G|$ of

DOI: 10.1021/acs.jpca.9b01937
J. Phys. Chem. A 2019, 123, 4034−4047

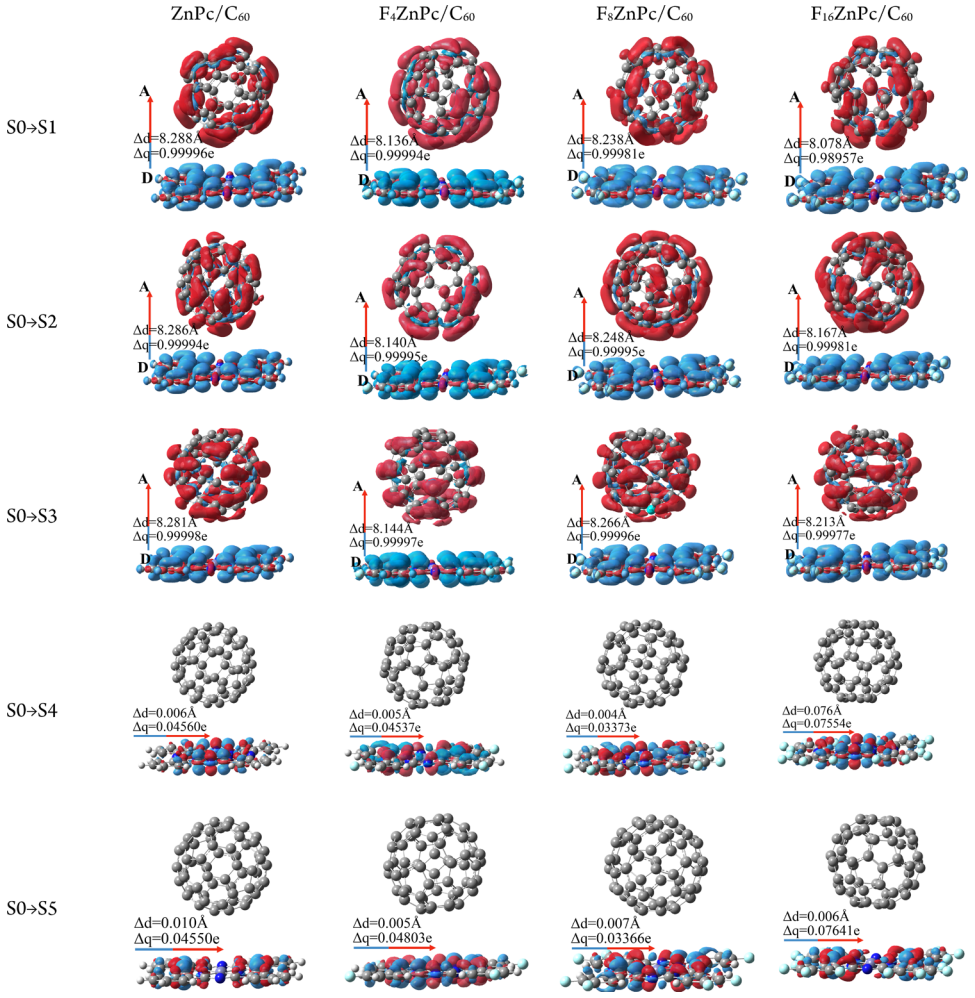

Figure 6. Charge density difference for the low-lying excited states of F_nZnPc/C_{60} (n = 0, 4, 8, 16) complexes. The regions colored in red and blue indicate the increase and the decrease of electron density during excitation processes, respectively. The charge transfer distance and the amount of charge transfer are shown.

$ZnPc/C_{60}$ for the CT process is slightly smaller than that of F_4ZnPc/C_{60}. Meanwhile, with increasing number of F atoms in F_nZnPc/C_{60} (n = 0, 4, 8, 16) and chlorination of $SubPc/C_{60}$ (n = 0, 6), the absolute values of $|\Delta G|$ for ED and CR processes decrease and increase, respectively. The smallest $|\Delta G|$ of ED for $F_{16}ZnPc/C_{60}$ means the absence of enough driving force for ED. Hence, generally, halogenation reduces the absolute values of the ΔG for the CT and ED processes and increases the ΔG for the CR process. According to computational methods, this is because the halogenation effects on IPD (see Table 5) are more significant than those on local excitation energies and exciton binding energies.

The total reorganization energy (λ_{total}) includes the internal and external reorganization energies. With an approximate external reorganization energy of 0.11 eV, the λ_{total} values are given in Table 6. The λ_{total} values of F_nZnPc/C_{60} (n = 0, 4, 8, 16) in the CT and ED processes were 0.42−0.50 and 0.42−0.48 eV, respectively, and were not monotonically dependent on the degree of fluorination. The λ_{total} of complex F_nZnPc/C_{60} (n = 0, 4, 8, 16) in the CR process is ∼0.2 eV less than those of the CT and ED processes, and the effect of halogenation is relatively obvious, which leads to increasing λ_{total} with the increase in n. The λ_{total} of the Cl_6SubPc/C_{60} complex is slightly larger than that of the $SubPc/C_{60}$ complex in the three processes. Similar to those of F_nZnPc/C_{60} (n = 0, 4, 8, 16) complexes, the λ_{total} values of CR for Cl_nSubPc/C_{60} (n = 0, 6) complexes are also ∼0.2 eV less than those of ED and CT processes. The λ_{total} of the $F_{16}ZnPc/C_{60}$ complex for CT, ED, and CR processes is the largest among these complexes. The increasing λ_{total} by halogenation is also supported by the case of perfluorination of polyacenes.[59,60] The λ_{total} of F_8ZnPc/C_{60} is very close to that of $ZnPc/C_{60}$. It can be attributed to the dependence of reorganization energy on the fluorination position. The similar case is the fluorination of ITIC.[61] Furthermore, the largest λ_{total} values of $F_{16}ZnPc/C_{60}$ and Cl_6SubPc/C_{60} complexes suggest that halogenation results in the significant variation of the potential energy surface for the donor's excited states and cation states relative to those for the ground states.

The electronic coupling V_{DA} values of the CT, ED, and CR processes are also listed in Table 6. The V_{DA} for the CT process is negatively correlated with the number of halogen atoms, decreasing from 2.00 to 1.33 meV for F_nZnPc/C_{60} (n = 0, 4, 8, 16) complexes and from 2.16 to 1.24 meV for $SubPc/C_{60}$ (n = 0, 6) complexes. Due to the importance of V_{DA} in Marcus theory, the V_{DA} reduction leads to a negative impact on the interface CT rate and ultimately to a decrease in carrier generation efficiency. On the contrary, the V_{DA} for the ED processes increase with the increase in number of F atoms in F_nZnPc/C_{60} (n = 0, 4, 8, 16) complexes, but it decreases after

DOI: 10.1021/acs.jpca.9b01937
J. Phys. Chem. A 2019, 123, 4034−4047

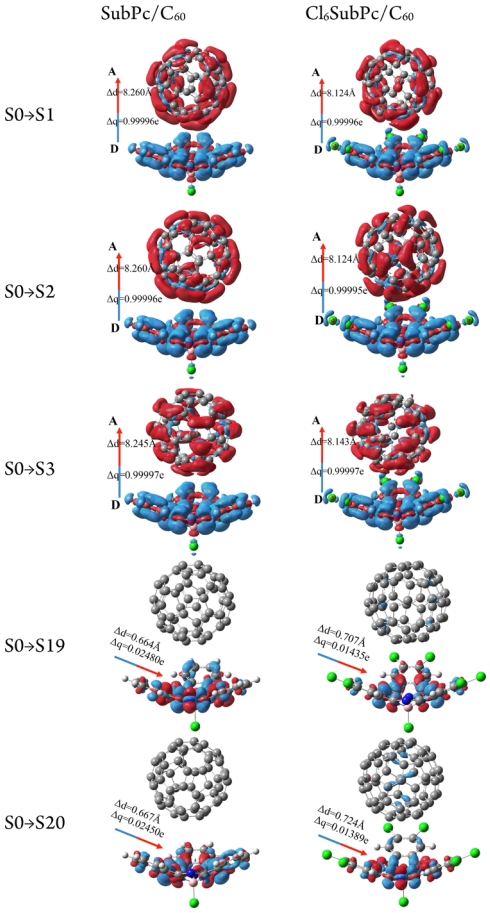

Figure 7. Charge density difference for the selected excited states of Cl_nSubPc/C_{60} (n = 0, 6) complexes. The regions colored in red and blue indicate the increase and the decrease of electron density during excitation processes, respectively. The charge transfer distance and the amount of charge transfer are shown.

Table 5. Calculated Ionization Potentials of the Donors IP_D, Electron Affinities of the Acceptor EA_A, Fundamental Gaps Defined as the Difference between the Ionization Energy of Donor and the Electron Affinity of Acceptor ($IP_D - EA_A$), First Adiabatic Excitation Energy of Donor E_{S1A}, and Exciton Binding Energy E_{exb} (in eV)

complex	IP_D	EA_A	$IP_D - EA_A$	E_{S1A}	E_{exb}
$ZnPc/C_{60}$	4.9215	3.2942	1.6272	1.8284	0.4032
F_4ZnPc/C_{60}	5.0892	3.2941	1.7951	1.8141	0.3848
F_8ZnPc/C_{60}	5.2418	3.2941	1.9478	1.8945	0.3821
$F_{16}ZnPc/C_{60}$	5.4562	3.2942	2.1620	1.8072	0.4039
$SubPc/C_{60}$	5.3032	3.2686	2.0346	2.2315	0.4583
Cl_6SubPc/C_{60}	5.6768	3.2686	2.4082	2.2099	0.4638

chlorination of $SubPc/C_{60}$ complexes, meaning that the V_{DA} for the ED processes can be enhanced by fluorination of ZnPc while it can be reduced by fluorination of SubPc. As for the CR process, the increase in number of halogen atoms enhances the V_{DA}, increasing from 0.7 to 25.34 meV for F_nZnPc/C_{60} (n = 0, 4, 8, 16) complexes and from 1.39 to 1.46 meV for Cl_6SubPc/C_{60} (n = 0, 6) complexes. In terms of the generalized Mulliken−Hush (GMH) model for calculating V_{DA},[62,63] the increase of the first excitation energy and the transition dipole moment is the main reason for the V_{DA} enhancement. The chlorination-induced increase of the optical band gap and the transition dipole moment was confirmed.[14]

For F_nZnPc/C_{60} (n = 0, 4, 8) and $SubPc/C_{60}$ (n = 0, 6) complexes, the photoinduced direct CT rates (in Table 6) decrease with the increase of halogenation degree. Since the relative differences of $|\Delta G + \lambda|$ among the complexes are smaller than those of the V_{DA}, the reason for the CT rate decrease mainly depends on the sequential decline of the V_{DA}.

Similarly, the rates of CR (in Table 6) processes decrease with increasing number of halogen atoms (except for $F_{16}ZnPc/C_{60}$). $F_{16}ZnPc/C_{60}$ is so special that its CR rate is 4 orders greater than that of F_8ZnPc/C_{60}, mainly because the former's electronic coupling is about 5 times that of the latter. Although the $|\Delta G + \lambda|$ of the F_8ZnPc/C_{60} complexes is smaller than that of $F_{16}ZnPc/C_{60}$ complexes, the dominating role of $|V_{DA}|$ results in a larger CR rate of $F_{16}ZnPc/C_{60}$ complexes.

The ED process rates (in Table 6) increase with the increasing degree of halogenation for F_nZnPc/C_{60} (n = 0, 4, 8) complexes except for the $F_{16}ZnPc/C_{60}$ complex. For the case of $F_{16}ZnPc/C_{60}$ complexes, the absolute value of $|\Delta G + \lambda|$ is relatively large, and the V_{DA} is at the same order as those of F_nZnPc/C_{60} (n = 0, 4, 8); thus, the dominant factor of $|\Delta G + \lambda|$ leads to the slower ED rate than those of F_nZnPc/C_{60} (n = 0, 4, 8) complexes. Hence, the less efficient ED is one possible reason for the worse performance of $F_{16}ZnPc/C_{60}$ bilayer OPV devices.[21]

For Cl_nSubPc/C_{60} (n = 0, 6) complexes, the ED rate of $SubPc/C_{60}$ is slightly larger, indicating the chlorination effect. The ED rate of 1.44×10^{10} s^{-1} of $SubPc/C_{60}$ in this work is slower than the experimental value (0.1 ps^{-1}) and theoretical value (2 ps^{-1}) based on a Fermi's golden rule approach.[28] Because the electron delocalization takes a positive role in the ED process,[64] the underestimation of the ED rate in this work can be improved by consideration of charge delocalization, which requires a more complex model and huge computational cost. On the other hand, the effect of halogenation on the dielectric constant was not considered, which may further enhance CT and ED rates and reduce the CR rate. This has been confirmed in a recent study where the fluorination of the acceptor leads to an increase in the dielectric constant of the donor/acceptor heterojunction, favoring the effective retardation of bimolecular recombination and the high charge dissociation rate and low geminate losses.[65] However, because the dielectric constants of organic optoelectronic materials are usually small (typical values are 3−5), the variation of dielectric constants induced by halogenation should not change excitation energies and other physical quantities remarkably.

4. CONCLUSIONS

Based upon quantum chemistry calculations of ωB97XD/6-311G(d,p) with optimally tuned range separation parameters and solid polarization effects, we studied the effects of donor halogenation on molecular geometries, electronic structures, excitation, and spectroscopic properties for F_nZnPc (n = 0, 4, 8, 16) and Cl_nSubPc (n = 0, 6) monomers and the complexes with C_{60}, which are selected as model systems, and the halogenation effects on photoinduced direct CT, ED, and CR process at the heterojunction interface were investigated by rate constants calculated using Marcus theory. The main conclusions are as follows:

DOI: 10.1021/acs.jpca.9b01937
J. Phys. Chem. A 2019, 123, 4034−4047

Table 6. Calculated Reorganization Energies λ (eV), Free Energy Changes ΔG (eV), Absolute Value of the Difference between Free Energy Change and Reorganization Energy $|\Delta G + \lambda|$ (eV), Electron Coupling V_{DA} (meV), and Rate Constants k (s^{-1}) of the Six Complexes for the Three Electron Transfer Processes (ETP including CT, ED, and CR)

complex	ETP	λ_{total} (λ_{out} = 0.11)	ΔG	$\lvert\Delta G + \lambda\rvert$	V_{DA}	k
$ZnPc/C_{60}$	CT	0.4429	−0.0703	0.3726	2.00	4.88×10^{9}
	ED	0.4330	−0.6044	0.1713	1.48	2.90×10^{10}
	CR	0.1968	−1.2240	1.0272	0.70	6.27×10^{-13}
F_4ZnPc/C_{60}	CT	0.4184	−0.0764	0.3420	1.59	4.40×10^{9}
	ED	0.4238	−0.4037	0.0201	2.54	1.64×10^{11}
	CR	0.2065	−1.4104	1.2039	1.10	1.68×10^{-19}
F_8ZnPc/C_{60}	CT	0.4299	−0.0622	0.3677	1.50	2.76×10^{9}
	ED	0.4208	−0.3289	0.0919	3.55	3.42×10^{11}
	CR	0.2074	−1.5657	1.3583	5.15	4.96×10^{-26}
$F_{16}ZnPc/C_{60}$	CT	0.4969	−0.0170	0.4799	1.33	4.78×10^{8}
	ED	0.4770	−0.0491	0.4279	4.17	1.04×10^{10}
	CR	0.2666	−1.7581	1.4915	25.34	2.20×10^{-22}
$SubPc/C_{60}$	CT	0.4148	−0.1535	0.2613	2.16	2.48×10^{10}
	ED	0.4233	−0.6552	0.2319	1.38	1.44×10^{10}
	CR	0.2307	−1.5763	1.3456	1.39	8.36×10^{-23}
Cl_6SubPc/C_{60}	CT	0.4316	−0.1422	0.2894	1.24	6.02×10^{9}
	ED	0.4303	−0.2655	0.1648	0.98	1.33×10^{10}
	CR	0.2392	−1.9444	1.7052	1.46	7.92×10^{-41}

i The very tiny differences of molecular geometries, H−L_{gap}, excitation, and spectroscopic properties among the F_nZnPc (n = 0, 4, 8, 16) and Cl_nSubPc (n = 0, 6) monomers point to the idea that these quantities are insensitive to halogenation, indicating that the electronic and optical gap cannot be effectively tuned by halogenation of F_nZnPc (n = 0, 4, 8, 16) and Cl_nSubPc (n = 0, 6). However, halogenation causes a significant decrease in energies of the HOMO and LUMO, leading to a remarkable influence on the energy level alignment at heterojunction interfaces, which is crucial for ED from localized excitons generated within donor layers to CT states at heterojunction interfaces, and it may further impact the OPV's working principle. In terms of tiny LUMO difference between $F_{16}ZnPc$ and C_{60}, it was suggested that $F_{16}ZnPc/C_{60}$ OPVs behave as Schottky cells.[21] Therefore, the halogenation degree may lead to the different working principles of OPV devices.

ii The halogenation enhances intermolecular binding energies between C_{60} and donors, and thus can improve the morphology regioregularity of donor/acceptor interfaces in OPV heterojunctions. Fluorination of ZnPc and chlorination of SubPc increase the CT excitation energies of F_nZnPc/C_{60} (n = 0, 4, 8, 16) and Cl_nSubPc/C_{60} (n = 0, 6) complexes. Hence, the fluorination of ZnPc and chlorination of SubPc can improve the V_{OC} of OPVs.

iii For F_nZnPc/C_{60} (n = 0, 4, 8, 16) and $SubPc/C_{60}$ (n = 0, 6) complexes, the photoinduced direct CT rates decrease with the increase of halogenation degree. The ED process rates increase with the increasing degree of halogenation for F_nZnPc/C_{60} (n = 0, 4, 8) complexes except for the $F_{16}ZnPc/C_{60}$ complex. The chlorination of SubPc generates a slight decrease of the ED rate. The rates of the CR processes dramatically decrease (several orders) with increasing number of halogen atoms (except for $F_{16}ZnPc/C_{60}$). Therefore, the reported PCE improvement induced by halogenation can be mainly ascribed to suppression of CR processes.

iv For the special case of $F_{16}ZnPc/C_{60}$, the slower ED and CT rates and the relative faster CR rate explain its worse OPV performance. This underlines the importance of fluorination degree in molecular design of donor materials because the degree of fluorination affects the rates of CT, ED, and CR.

The results of this work could be helpful to understand the different photovoltaic performances of halogenated donor materials, which is favorable for molecular design of novel donor materials with the aid of halogenation.

■ ASSOCIATED CONTENT

Supporting Information

The Supporting Information is available free of charge on the ACS Publications website at DOI: 10.1021/acs.jpca.9b01937.

Optimized geometric parameters of monomers and complexes and their excited states and molecular orbital maps and electric quadrupole moment of the monomers (PDF)

■ AUTHOR INFORMATION

Corresponding Author

*E-mail: zhcrxy@lut.cn. Phone: +86 0931 2973780. Fax: +86 0931 2976040.

Notes

The authors declare no competing financial interest.

■ ACKNOWLEDGMENTS

This work was supported by the National Natural Science Foundation of China (grant no. 11164016) and the HongLiu First-class disciplines Development Program of Lanzhou University of Technology. C.-R.Z. thanks Prof. Yuanping Yi (CAS) for electronic coupling calculations. The authors were grateful to the Gansu Computing Center and the National Supercomputing Center in Shenzhen and Changsha.

DOI: 10.1021/acs.jpca.9b01937
J. Phys. Chem. A 2019, 123, 4034−4047

REFERENCES

(1) Meng, L.; Zhang, Y.; Wan, X.; Li, C.; Zhang, X.; Wang, Y.; Ke, X.; Xiao, Z.; Ding, L.; Xia, R.; et al. Organic and Solution-Processed Tandem Solar Cells with 17.3% Efficiency. *Science* **2018**, *361*, 1094.

(2) Xiao, S.; Zhang, Q.; You, W. Molecular Engineering of Conjugated Polymers for Solar Cells: An Updated Report. *Adv. Mater.* **2017**, *29*, 1601391.

(3) Brédas, J.-L.; Norton, J. E.; Cornil, J.; Coropceanu, V. Molecular Understanding of Organic Solar Cells: The Challenges. *Acc. Chem. Res.* **2009**, *42*, 1691−1699.

(4) Lu, L.; Kelly, M. A.; You, W.; Yu, L. Status and Prospects for Ternary Organic Photovoltaics. *Nat. Photonics* **2015**, *9*, 491.

(5) Nam, M.; Cha, M.; Lee, H. H.; Hur, K.; Lee, K.-T.; Yoo, J.; Han, I. K.; Kwon, S. J.; Ko, D.-H. Long-Term Efficient Organic Photovoltaics Based on Quaternary Bulk Heterojunctions. *Nat. Commun.* **2017**, *8*, 14068.

(6) Zhao, W.; Li, S.; Yao, H.; Zhang, S.; Zhang, Y.; Yang, B.; Hou, J. Molecular Optimization Enables over 13% Efficiency in Organic Solar Cells. *J. Am. Chem. Soc.* **2017**, *139*, 7148−7151.

(7) Kan, B.; Zhang, J.; Liu, F.; Wan, X.; Li, C.; Ke, X.; Wang, Y.; Feng, H.; Zhang, Y.; Long, G.; Friend, R. H.; et al. Fine-Tuning the Energy Levels of a Nonfullerene Small-Molecule Acceptor to Achieve a High Short-Circuit Current and a Power Conversion Efficiency over 12% in Organic Solar Cells. *Adv. Mater.* **2018**, *30*, 1704904.

(8) Zhou, Y.; Kurosawa, T.; Ma, W.; Guo, Y.; Fang, L.; Vandewal, K.; Diao, Y.; Wang, C.; Yan, Q.; Reinspach, J.; et al. High Performance All-Polymer Solar Cell via Polymer Side-Chain Engineering. *Adv. Mater.* **2014**, *26*, 3767−72.

(9) Ji, Z.; Xu, X.; Zhang, G.; Li, Y.; Peng, Q. Synergistic effect of Halogenation on Molecular Energy Level and Photovoltaic Performance Modulations of Highly Efficient Small Molecular Materials. *Nano Energy* **2017**, *40*, 214−223.

(10) Zhang, Y.; Yao, H.; Zhang, S.; Qin, Y.; Zhang, J.; Yang, L.; Li, W.; Wei, Z.; Gao, F.; Hou, J. Fluorination vs. Chlorination: a Case Study on High Performance Organic Photovoltaic Materials. *Sci. China-Chem.* **2018**, *61*, 1328−1337.

(11) Zhang, S.; Qin, Y.; Zhu, J.; Hou, J. Over 14% Efficiency in Polymer Solar Cells Enabled by a Chlorinated Polymer Donor. *Adv. Mater.* **2018**, *30*, 1800868.

(12) Chen, H.; Hu, Z.; Wang, H.; Liu, L.; Chao, P.; Qu, J.; Chen, W.; Liu, A.; He, F. A Chlorinated π-Conjugated Polymer Donor for Efficient Organic Solar Cells. *Joule* **2018**, *2*, 1623−1634.

(13) Liu, Z.; Gao, Y.; Dong, J.; Yang, M.; Liu, M.; Zhang, Y.; Wen, J.; Ma, H.; Gao, X.; Chen, W.; et al. Chlorinated Wide-Bandgap Donor Polymer Enabling Annealing Free Nonfullerene Solar Cells with the Efficiency of 11.5%. *J. Phys. Chem. Lett.* **2018**, *9*, 6955−6962.

(14) Zhao, Z.-W.; Pan, Q.-Q.; Geng, Y.; Wu, S.-X.; Zhang, M.; Zhao, L.; Su, Z.-M. A Theorectical Design of Performant Chlorinated Benzothiadiazole-Based Polymers as Donor for Organic Photovoltaic Devices. *Org. Electron.* **2018**, *61*, 46−55.

(15) Ashokan, A.; Wang, T.; Ravva, M. K.; Brédas, J.-L. Impact of Solution Temperature-Dependent Aggregation on the Solid-State Packing and Electronic Properties of Polymers for Organic Photovoltaics. *J. Mater. Chem. C.* **2018**, *6*, 13162−13170.

(16) Chen, H. Y.; Hou, J.; Zhang, S.; Liang, Y.; Yang, G.; Yang, Y.; Yu, L.; Wu, Y.; Li, G. Polymer Solar Cells with Enhanced Open-circuit Voltage and Efficiency. *Nat. Photonics* **2009**, *3*, 649−653.

(17) Price, S. C.; Stuart, A. C.; Yang, L.; Zhou, H.; You, W. Fluorine Substituted Conjugated Polymer of Medium Band Gap Yields 7% Efficiency in Polymer−Fullerene Solar Cells. *J. Am. Chem. Soc.* **2011**, *133*, 4625−4631.

(18) Zhou, H.; Yang, L.; Stuart, A. C.; Price, S. C.; Liu, S.; You, W. Development of Fluorinated Benzothiadiazole as a Structural Unit for a Polymer Solar Cell of 7% Efficiency. *Angew. Chem. Int. Edit.* **2011**, *50*, 2995−8.

(19) Zhang, S.; Qin, Y.; Uddin, M. A.; Jang, B.; Zhao, W.; Liu, D.; Woo, H. Y.; Hou, J. A Fluorinated Polythiophene Derivative with Stabilized Backbone Conformation for Highly Efficient Fullerene and Non-Fullerene Polymer Solar Cells. *Macromol.* **2016**, *49*, 2993−3000.

(20) Schwarze, M.; Tress, W.; Beyer, B.; Gao, F.; Scholz, R.; Poelking, C.; Ortstein, K.; Gunther, A. A.; Kasemann, D.; Andrienko, D.; et al. Band Structure Engineering in Organic Semiconductors. *Science* **2016**, *352*, 1446−9.

(21) Brendel, M.; Krause, S.; Steindamm, A.; Topczak, A. K.; Sundarraj, S.; Erk, P.; Höhla, S.; Fruehauf, N.; Koch, N.; Pflaum, J. The Effect of Gradual Fluorination on the Properties of FnZnPc Thin Films and FnZnPc/C_{60} Bilayer Photovoltaic Cells. *Adv. Funct. Mater.* **2015**, *25*, 1565−1573.

(22) Meiss, J.; Merten, A.; Hein, M.; Schuenemann, C.; Schäfer, S.; Tietze, M.; Uhrich, C.; Pfeiffer, M.; Leo, K.; Riede, M. Fluorinated Zinc Phthalocyanine as Donor for Efficient Vacuum-Deposited Organic Solar Cells. *Adv. Funct. Mater.* **2012**, *22*, 405−414.

(23) Mutolo, K. L.; Mayo, E. I.; Rand, B. P.; Forrest, S. R.; Thompson, M. E. Enhanced Open-Circuit Voltage in Subphthalocyanine/C_{60} Organic Photovoltaic Cells. *J. Am. Chem. Soc.* **2006**, *128*, 8108−9.

(24) Pandey, R.; Gunawan, A. A.; Mkhoyan, K. A.; Holmes, R. J. Efficient Organic Photovoltaic Cells Based on Nanocrystalline Mixtures of Boron Subphthalocyanine Chloride and C_{60}. *Adv. Funct. Mater.* **2012**, *22*, 617−624.

(25) Lee, M. H.; Geva, E.; Dunietz, B. D. Calculation from First-Principles of Golden Rule Rate Constants for Photoinduced Subphthalocyanine/Fullerene Interfacial Charge Transfer and Recombination in Organic Photovoltaic Cells. *J. Phys. Chem. C* **2014**, *118*, 9780−9789.

(26) Sato, K.; Pradhan, E.; Asahi, R.; Akimov, A. V. Charge Transfer Dynamics at The Boron Subphthalocyanine chloride/C_{60} interface: Non-Adiabatic Dynamics Study with Libra-X. *Phys. Chem. Chem. Phys.* **2018**, *20*, 25275−25294.

(27) Lee, M. H.; Geva, E.; Dunietz, B. D. The Effect of Interfacial Geometry on Charge-Transfer States in the Phthalocyanine/Fullerene Organic Photovoltaic System. *J. Phys. Chem. A.* **2016**, *120*, 2970−5.

(28) Wilcox, D. E.; Lee, M. H.; Sykes, M. E.; Niedringhaus, A.; Geva, E.; Dunietz, B. D.; Shtein, M.; Ogilvie, J. P. Ultrafast Charge-Transfer Dynamics at the Boron Subphthalocyanine Chloride/C_{60} Heterojunction: Comparison between Experiment and Theory. *J. Phys. Chem. Lett.* **2015**, *6*, 569−75.

(29) Mihailetchi, V. D.; Koster, L. J. A.; Hummelen, J. C.; Blom, P. W. M. Photocurrent Generation in Polymer-Fullerene Bulk Heterojunctions. *Phys. Rev. Lett.* **2004**, *93*, 216601.

(30) Vandewal, K.; Albrecht, S.; Hoke, E. T.; Graham, K. R.; Widmer, J.; Douglas, J. D.; Schubert, M.; Mateker, W. R.; Bloking, J. T.; Burkhard, G. F.; Sellinger, A.; et al. Efficient Charge Generation by Relaxed Charge-Transfer States at Organic Interfaces. *Nat. Mater.* **2014**, *13*, 63.

(31) Rand, B. P.; Cheyns, D.; Vasseur, K.; Giebink, N. C.; Mothy, S.; Yi, Y.; Coropceanu, V.; Beljonne, D.; Cornil, J.; Brédas, J.-L.; et al. The Impact of Molecular Orientation on the Photovoltaic Properties of a Phthalocyanine/Fullerene Heterojunction. *Adv. Funct. Mater.* **2012**, *22*, 2987−2995.

(32) Jailaubekov, A. E.; Willard, A. P.; Tritsch, J. R.; Chan, W.-L.; Sai, N.; Gearba, R.; Kaake, L. G.; Williams, K. J.; Leung, K.; Rossky, P. J.; Zhu, X. Y.; et al. Hot Charge-Transfer Excitons Set the Time Limit for Charge Separation at Donor/Acceptor Interfaces in Organic Photovoltaics. *Nat. Mater.* **2013**, *12*, 66.

(33) Marcus, R. A. Electron Transfer Reactions in Chemistry. Theory and Experiment. *Rev. Mod. Phys.* **1993**, *65*, 599−610.

(34) Frisch, M. J.; Pople, J. A.; Binkley, J. S. Self-Consistent Molecular Orbital Methods 25. Supplementary Functions for Gaussian Basis Sets. *J. Chem. Phys.* **1984**, *80*, 3265−3269.

(35) Chai, J.-D.; Head-Gordon, M. Long-Range Corrected Hybrid Density Functionals with Damped Atom−Atom Dispersion Corrections. *Phys. Chem. Chem. Phys.* **2008**, *10*, 6615−6620.

(36) Marenich, A. V.; Cramer, C. J.; Truhlar, D. G. Universal Solvation Model Based on Solute Electron Density and on a Continuum Model of the Solvent Defined by the Bulk Dielectric Constant and Atomic Surface Tensions. *J. Phys. Chem. B.* **2009**, *113*, 6378−96.

DOI: 10.1021/acs.jpca.9b01937
J. Phys. Chem. A 2019, 123, 4034−4047

(37) Kaur, M.; Kumar, R.; Dogra, R.; Arora, N.; Sharma, N. Characterization and Dielectric Properties of Vacuum-Deposited Zinc Phthalocyanine Thin Film. *Surf. Innov.* **2017**, *6*, 63−70.
(38) Saad, E. A. Effect of Phase Change on Dielectric Properties of Zinc Phthalocyanine Thin Films. *J. Optoelectron. Adv. M.* **2005**, *7*, 3127−3134.
(39) Morse, G. E.; Bender, T. P. Boron Subphthalocyanines as Organic Electronic Materials. *ACS Appl. Mater. Inter.* **2012**, *4*, 5055−5068.
(40) Singh, M.; Mahajan, A.; Gupta, N.; Bedi, R. K. Study of Junction Charge Transport Properties of Boron Subphthalocyanine Chloride Thin Film. *Electron. Mater. Lett.* **2015**, *11*, 118−126.
(41) Chen, X. K.; Ravva, M. K.; Li, H.; Ryno, S. M.; Brédas, J. L. Effect of Molecular Packing and Charge Delocalization on the Nonradiative Recombination of Charge-Transfer States in Organic Solar Cells. *Adv. Energy Mater.* **2016**, *6*, 1601325.
(42) Marenich, A. V.; Cramer, C. J.; Truhlar, D. G.; Guido, C. A.; Mennucci, B.; Scalmani, G.; Frisch, M. J. Practical Computation of Electronic Excitation in Solution: Vertical Excitation Model. *Chem. Sci.* **2011**, *2*, 2143−2161.
(43) Molbase, *Chemical B2B E-Commerce Platform*. http://www.molbase.com/cas/99685-96-8.html.
(44) Baer, R.; Livshits, E.; Salzner, U. Tuned Range-Separated Hybrids in Density Functional Theory. *Annu. Rev. Phys. Chem.* **2010**, *61*, 85−109.
(45) Stein, T.; Kronik, L.; Baer, R. Prediction of Charge-Transfer Excitations in Coumarin-Based Dyes Using a Range-Separated Functional Tuned from First Principles. *J. Chem. Phys.* **2009**, *131*, 244119.
(46) Frisch, M.; Trucks, G.; Schlegel, H.; Scuseria, G.; Robb, M.; Cheeseman, J.; Scalmani, G.; Barone, V.; Mennucci, B.; Petersson, G. A. et al. *Gaussian 09*, Revision D. 01; Gaussian Inc.: Wallingford CT, 2009.
(47) Lu, T.; Chen, F. Multiwfn: A Multifunctional Wavefunction Analyzer. *J. Comput. Chem.* **2012**, *33*, 580−592.
(48) Lu, T. *Multiwfn Manual*, version 3.6(dev), Section 3.21.1, 3.21.8,available at http://sobereva.com/multiwfn
(49) Landi, A.; Borrelli, R.; Capobianco, A.; Velardo, A.; Peluso, A. Hole Hopping Rates in Organic Semiconductors: A Second-Order Cumulant Approach. *J. Chem. Theory Comput.* **2018**, *14*, 1594−1601.
(50) Bai, R.-R.; Zhang, C.-R.; Wu, Y.-Z.; Yuan, L.-H.; Zhang, M.-L.; Chen, Y.-H.; Liu, Z.-J.; Chen, H.-S. The Interface Configuration Effects on Excitation Properties, Exciton Dissociation and Charge Recombination in Organic Photovoltaic Heterojunction: The Case of P-SIDT$(FBTTh_2)_2$/C_{60} Complexes, submitted for publication.
(51) Sullivan, P.; Duraud, A.; Hancox, l.; Beaumont, N.; Mirri, G.; Tucker, J. H. R.; Hatton, R. A.; Shipman, M.; Jones, T. S. Halogenated Boron Subphthalocyanines as Light Harvesting Electron Acceptors in Organic Photovoltaics. *Adv. Energy Mater.* **2011**, *1*, 352−355.
(52) Beaumont, N.; Castrucci, J. S.; Sullivan, P.; Morse, G. E.; Paton, A. S.; Lu, Z. H.; Bender, T. P.; Jones, T. S. Acceptor Properties of Boron Subphthalocyanines in Fullerene Free Photovoltaics. *J. Phys. Chem. C* **2014**, *118*, 14813−14823.
(53) Kalia, S.; Mahajan, A.; Ghansyam, C. G.; Debnath, A. K.; Saxsena, V.; Aswal, D. K.; Bedi, R. K. Anisotropic Charge Transport Properties in Boron Sub Phthalocyanine Chloride Thin Films. *J. Appl. Phys.* **2017**, *121*, No. 095501.
(54) Pan, Q.-Q.; Li, S.-B.; Wu, Y.; Geng, Y.; Zhang, M.; Su, Z.-M. Exploring More Effective Polymer Donors for the Famous Non-Fullerene Acceptor ITIC in Organic Solar Cells by Increasing Electron-Withdrawing Ability. *Org. Electron.* **2018**, *53*, 308−314.
(55) Zhang, C.-R.; Sears, J. S.; Yang, B.; Aziz, S. G.; Coropceanu, V.; Brédas, J.-L. Theoretical Study of the Local and Charge-Transfer Excitations in Model Complexes of Pentacene-C_{60} Using Tuned Range-Separated Hybrid Functionals. *J. Chem. Theory Comput.* **2014**, *10*, 2379−2388.
(56) Yi, Y.; Coropceanu, V.; Brédas, J.-L. Exciton-Dissociation and Charge-Recombination Processes in Pentacene/C_{60} Solar Cells: Theoretical Insight into the Impact of Interface Geometry. *J. Am. Chem. Soc.* **2009**, *131*, 15777−15783.
(57) Ren, J.; Meng, S.; Kaxiras, E. Theoretical Investigation of The C_{60}/Copper Phthalocyanine Organic Photovoltaic Heterojunction. *Nano Res.* **2012**, *5*, 248−257.
(58) Morse, G. E.; Gantz, J. L.; Steirer, K. X.; Armstrong, N. R.; Bender, T. P. Pentafluorophenoxy Boron Subphthalocyanine (F_5BsubPc) as a Multifunctional Material for Organic Photovoltaics. *ACS Appl. Mater. Interfaces* **2014**, *6*, 1515−1524.
(59) Chen, H.-Y.; Chao, I. Effect of Perfluorination on the Charge-Transport Properties of Organic Semiconductors: Density Functional Theory Study of Perfluorinated Pentacene and Sexithiophene. *Chem. Phys. Lett.* **2005**, *401*, 539−545.
(60) Delgado, M. C. R.; Pigg, K. R.; da Silva Filho, D. A.; Gruhn, N. E.; Sakamoto, Y.; Suzuki, T.; Osuna, R. M.; Casado, J.; Hernández, V.; Navarrete, J. T. L.; et al. Impact of Perfluorination on the Charge-Transport Parameters of Oligoacene Crystals. *J. Am. Chem. Soc.* **2009**, *131*, 1502−1512.
(61) Han, G.; Guo, Y.; Ning, L.; Yi, Y. Improving the Electron Mobility of ITIC by End-Group Modulation: The Role of Fluorination and π-Extension. *Sol. RRL* **2019**, *3*, 1800251.
(62) Cave, R. J.; Newton, M. D. Generalization of the Mulliken-Hush Treatment for the Calculation of Electron Transfer Matrix Elements. *Chem. Phys. Lett.* **1996**, *249*, 15−19.
(63) Voityuka, A. A. Estimation of Electronic Coupling in π-stacked Donor-Bridge-Acceptor Systems: Correction of the Two-State Model. *J. Chem. Phys.* **2006**, *124*, No. 064505.
(64) Kahle, F. J.; Saller, C.; Olthof, S.; Li, C.; Lebert, J.; Weiss, S.; Herzig, E. M.; Huttner, S.; Meerholz, K.; Strohriegl, P.; Köhler, A.; et al. Does Electron Delocalization Influence Charge Separation at Donor-Acceptor Interfaces in Organic Photovoltaic Cells? *J. Phys. Chem. C* **2018**, *122*, 21792−21802.
(65) Zhang, X.; Zhang, D.; Zhou, Q.; Wang, R.; Zhou, J.; Wang, J.; Zhou, H.; Zhang, Y. Fluorination with an Enlarged Dielectric Constant Prompts Charge Separation and Reduces Bimolecular Recombination in Non-Fullerene Organic Solar Cells with a High Fill Factor and Efficiency > 13%. *Nano Energy* **2019**, *56*, 494−501.

DOI: 10.1021/acs.jpca.9b01937
J. Phys. Chem. A 2019, 123, 4034−4047